Analyst

PAPER

View Article Online
View Journal

Cite this: DOI: 10.1039/d3an01510f

Multiplexed electrical detection of whole viruses from plasma in a microfluidic platform†

Aaron Jankelow,[a,b,c] Chih-Lin Chen,[d] Thomas W. Cowell,[d] Javier Espinosa de los Monteros,[a,c] Zheng Bian,[a,b] Victoria Kindratenko,[a,b] Katherine Koprowski,[a,b] Sriya Darsi,[a,b] Hee-Sun Han,[d,e] Enrique Valera *[a,b,c,e] and Rashid Bashir *[a,b,c,e,f,g,h,i]

Received 1st September 2023,
Accepted 12th December 2023

DOI: 10.1039/d3an01510f

rsc.li/analyst

The advancement of point-of-care diagnostics is crucial to improving patient outcomes, especially in areas with low access to hospitals or specialized laboratories. In particular, rapid, sensitive, and multiplexed detection of disease biomarkers has great potential to achieve accurate diagnosis and inform high quality care for patients. Our Coulter counting and immunocapture based detection system has previously shown its broad applicability in the detection of cells, proteins, and nucleic acids. This paper expands the capability of the platform by demonstrating multiplexed detection of whole-virus particles using electrically distinguishable hydrogel beads by demonstrating the capability of our platform to achieve simultaneous detection at clinically relevant concentrations of hepatitis A virus (>2 × 10^3 IU mL^{-1}) and human parvovirus B19 virus like particles (>10^6 IU mL^{-1}) from plasma samples. The expanded versatility of the differential electrical counting platform allows for more robust and diverse testing capabilities.

1. Introduction

Delivering rapid and accurate diagnostics can be crucial to providing better patient outcomes and improving disease management. Point-of-care technologies that do not require expensive, bulky laboratory equipment and do not need highly trained operators can allow for these diagnostics to be more readily accessible in low-resource areas and lead to a faster response time for patient care. Current diagnostics for viruses tend to focus on either nucleic acid-based methods (*e.g.* PCR) or immunoassay-based diagnostics (*e.g.* ELISA).[1] Polymerase chain reaction (PCR) tests are highly sensitive however, they require bulky equipment for temperature cycling which are not well suited for the point-of-care (PoC). Much research is being done on other isothermal nucleic acid amplification techniques such as loop-mediated isothermal amplification (LAMP) and recombinase polymerase amplification (RPA) as alternatives to PCR to help alleviate this issue, however, these techniques have limited ability to acquire true simultaneous multiplexing without partitioning samples into multiple individual reactions that are performed separately, or utilizing fluorophores with different colors that may be hard to distinguish on a PoC device.[2–5] The other option is immunoassays, which can be used to detect either anti-viral antibodies or viral antigens.[1] The current gold standard for immunoassays are the enzyme-linked immunosorbent assays (ELISA), however these can take several hours to complete and requires bulky laboratory equipment making it hard to adapt for PoC applications and limited in its ability to achieve a speedy diagnosis.[1] Other methods for testing viral antigen particles like lateral flow assays can provide speedier diagnostics, but at the cost of lower sensitivity and an inability to make quantitative measurements as opposed to simple positive/negative readout.[1] On the other hand, immunoassay-based diagnostics for detection of antibodies are limited by the fact that endogenous antibodies are not present during early stages of infection, taking upwards of a week to appear post-infection.[6,7] Also, antibodies may not be present at all in some infected

[a]Department of Bioengineering, University of Illinois at Urbana-Champaign, Urbana, IL, 61801, USA. E-mail: evalerac@illinois.edu, rbashir@illinois.edu
[b]Nick Holonyak Jr Micro and Nanotechnology Laboratory, University of Illinois at Urbana-Champaign, Urbana, IL, 61801, USA
[c]Biomedical Research Center, Carle Foundation Hospital, Urbana, Illinois, USA
[d]Department of Chemistry, University of Illinois at Urbana-Champaign, Urbana, IL, 61801, USA
[e]Carl R. Woese Institute for Genomic Biology, University of Illinois at Urbana-Champaign, Urbana, Illinois, USA
[f]Department of Biomedical and Translation Science, Carle Illinois College of Medicine, University of Illinois at Urbana-Champaign, Urbana, IL, 61801, USA
[g]Department of Electrical and Computer Engineering, University of Illinois at Urbana-Champaign, Urbana, IL, 61801, USA
[h]Department of Mechanical Science and Engineering, University of Illinois at Urbana-Champaign, Urbana, IL, 61801, USA
[i]Department of Materials Science and Engineering, University of Illinois at Urbana-Champaign, Urbana, IL, 61801, USA
† Electronic supplementary information (ESI) available. See DOI: https://doi.org/10.1039/d3an01510f

individuals who do not develop immunity.[6,8,9] As such, there is a need to continue research into alternative approaches for virus detection in order to realize for more comprehensive, robust, and versatile diagnostics.

Multiplexed detection is a particular area of interest in expanding diagnostic capabilities because many conditions can have overlapping symptoms and some diseases may have increased complications upon concurrent infection.[1,4,10–12] Most multiplexed virus detections are performed through optical transducers. For example, multiplexed detection of up to 4 viruses in a single pot has been achieved using LAMP amplification techniques,[5,13] however the need for fluorescent labeling limits the degree of multiplexing that can be possible at PoC since differentiating more than 2–3 colors can be difficult to achieve without more precise equipment that may be prohibitive for these use cases. Additionally, false positives can be a problem when working with multiplexed LAMP due to the high number of primers (4–6 primers per target) required and designing primers to alleviate this issue can be a challenge.[5] Multiplexed lateral flow assays have been made for a number of conditions, however they rely on colorimetric readouts that are not capable of giving more information than positive/negative readouts.[14–16] Another optical approach to multiplexed virus detection involves using graphene-based biosensors to detect viral DNA without amplification, but attempts at multiplexed graphene sensors have had difficulty achieving low limits of detection, and also rely on fluorophores for multiplexing which once again lowers their usability in point-of-care devices.[11,17] As such, new methods of simultaneous multiplexing that are compatible with point-of-care testing are needed.

Electrical and electrochemical multiplexing techniques have also been worked on and provide advantages such as simpler instrumentation and being easier to miniaturize for point-of-care technologies.[18,19] Multiplexed detection of different strains influenza A virus has been demonstrated,[20] however similar to issues with optical detection, this required separate compartmentalization for each target (and spatial separation of the sample) and thus more complicated electrical instrumentations would be needed to keep expanding to a wider range of targets. Similarly a graphene-based platform for the multiplexed electrochemical detection of SARS-CoV-2 antibodies, antigens, and CRP was developed, but relied on individual working electrodes for each target.[21] Another issue these sensors face is that while they have provided success at targeting small analytes, they face issues with larger particles which diffuse slower and thus are less suitable for the detection of whole viral particles, which may limit useful applications.[22]

In previous studies, we showed the potential of our differential electrical counting platform to detect protein biomarkers,[23–25] cell surface biomarkers,[26,27] and nucleic acid targets.[25] We have also shown the potential of this technology to achieve multiplexed detection by incorporating multiple bead types each with distinct electrical impedance signals and functionalized with antibodies or DNA sequences specific to different targets in order to obtain multiplexed detection of both proteins and nucleic acids.[23,25] The foundational principle of this technology is differential Coulter counting, which is used to detect and enumerate cells and micro-sized beads as they move through counting electrodes before and after a capture chamber. Using an immunoassay on the surface of the particles and functionalizing the capture chambers with antibodies or streptavidin, targets are specifically captured on the beads, and the percentage of capture of each bead population can be correlated to the concentration of its target in the initial solution. The label-free nature of this platform allows for high multiplexing potential since we can produce a wide range of beads with distinct electrical signals with relatively small adjustments to the size and composition of hydrogel beads.[25] Additionally, because the beads can easily be swapped out for ones containing other targets, it allows for more flexible assays where targets could theoretically be mixed and matched at well with the same instrumentation, compared to multiplexed solutions that rely on compartmentalization and thus must be replaced entirely to diagnose different targets. Here we seek to expand the capabilities of this platform even further by demonstrating our ability to use it to capture and detect multiple whole virus particles without sample pretreatment such as chemical or thermal lysis or nucleic acid purification.

Hepatitis A virus (HAV) causes an inflammation of the liver, and while many cases are not fatal, it still infects thousands of people each year, with over 7000 deaths in 2016.[28] It causes epidemics periodically, such as one in Shanghai in 1988 that affected about 300 000 people.[28] The virus spreads mostly in poor and middle-income countries and cannot be diagnosed distinct from other viral hepatitis diseases without the use of specific tests.[28] Human parvovirus B19 (B19V) on the other hand is a common virus that has high infection rates around the world. Most cases are in children, however infection rates continue for adults later in life and infections in pregnant women can lead to complications such as miscarriage or hydrops fetalis.[8] While most cases are asymptomatic or present only mild symptoms, the virus is known to have more severe outcomes when it infects immunocompromised individuals such as those infected with HIV.[6–8,29] Both viruses have relatively simple structures, with HAV being an RNA virus with an ~30 nm diameter capsid composed of a single polyprotein which can be subdivided into 3 structural proteins,[30] and B19V is a DNA virus consisting of a 28 nm diameter capsid of two distinct viral proteins, VP1 and VP2, of which VP2 composes about 95% of the capsid.[31] The fact that both viruses have compelling reasons to want to use them for multiplexed testing, alongside the relative simplicity of their viral structures made them good candidates for an initial look into our platform's ability to achieve multiplexed detection of whole viruses.

In this study, we show our ability to expand the library of possible targets that can be detected with this platform by demonstrating its ability to achieve multiplexed capture and detection of whole HAV and B19V particles from plasma at

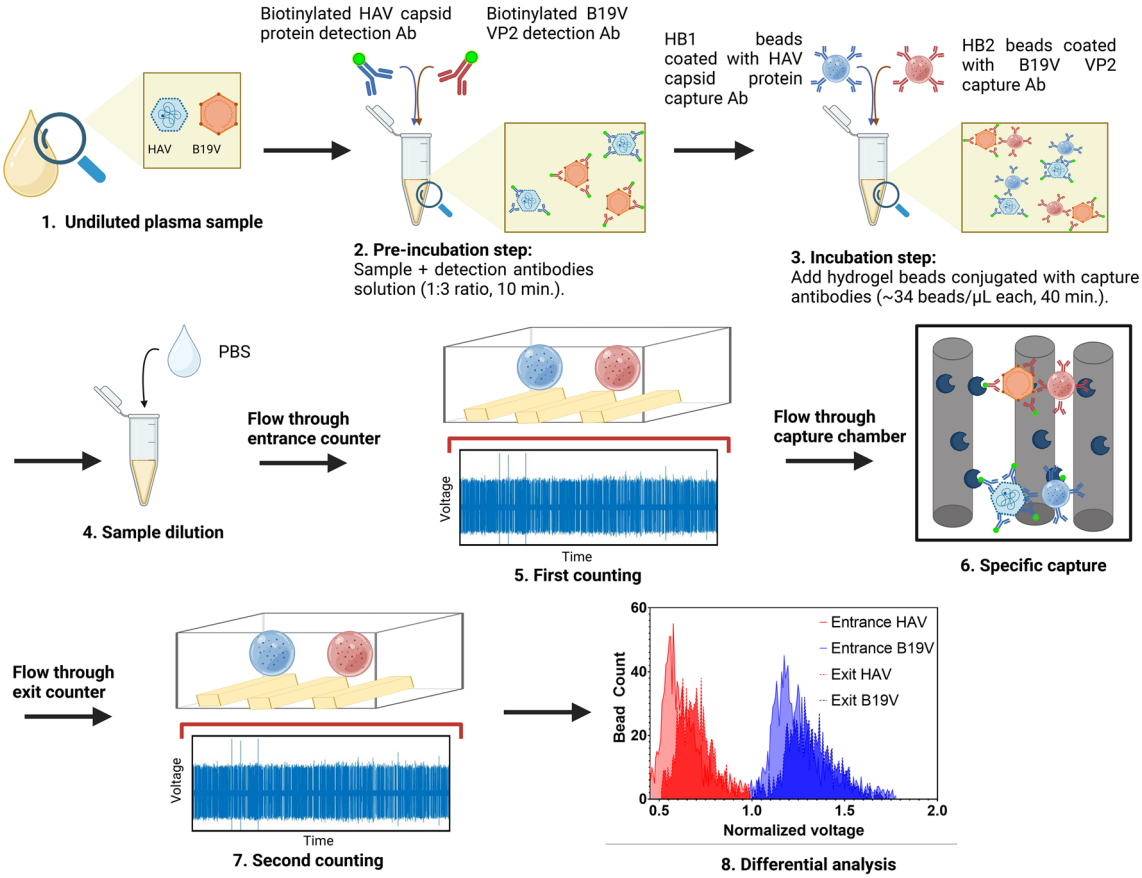

Fig. 1 Overview of the platform for the multiplexed detection of viral particles. A plasma sample is mixed with biotinylated detection antibodies solution (1 : 3 v/v ratio, preincubated for 10 min) to form a complex of virus coated in biotinylated antibody if the target is present in the sample. Two distinct types of hydrogel beads coated with the capture antibodies for each virus are then introduced (incubated for 40 min) to form a complex of bead-Ab1-virus-Ab2. This is then flowed through an entrance electrode to produce an entrance count before entering a capture chamber where beads that formed that full complex with virus are specifically captured on posts functionalized with streptavidin. The beads that have not been captured then flow through an exit electrode to get an exit count. The count data is analyzed in MATLAB and a differential count is obtained to calculate the percentage of capture. Image created with Biorender.

clinically relevant levels. With this work, we aimed to demonstrate an approach that could detect the viruses simultaneously, in a short time and at clinically relevant levels, opening the door to the early detection of infections caused by these pathogens. The overview of our multiplexed device can be seen in Fig. 1. By expanding the potential targets that can be detected with this platform, we increase its versatility allowing for more varied and robust diagnostic applications.

The intent of this microfluidic device is to provide a solution that can be used out of centralized laboratories, such as those at the primary care or emergency level, where the rapid detection and identification of viruses can contribute to prevention of transmission to the community. In comparison to other electrical and electrochemical multiplexing techniques where spatial separation of the sample is needed or individual working electrodes for each target are needed, our device's instrumentation and complexity does not change by adding more hydrogel beads to increase the level of multiplexing. In this work we demonstrate the ability of our microfluidic platform to achieve multiplexed capture and detection of whole viral particles in plasma samples. Future work with focus on incorporation of the entire assay, from mixing to detection, into an integrated portable device.

2. Materials and methods

2.1. Chemicals and reagents

HAV antibodies without biotin (Cat# DMABT-51306MH) and formaldehyde-inactivated HAV viral particles (Cat# DAG178) were obtained from Creative Diagnostics. Biotinylated HAV antibodies (Cat# LS-C526508-100) as well as biotinylated (Cat# LS-C371159-100) and nonbiotinylated (Cat# LS-C371157-100) antibodies for B19V VP2 antigen were purchased from Lifespan Biosciences. EDC (Cat# 22980) and Sulfo-NHS (Cat# 21326) were obtained from Thermo Fisher Scientific. B19V virus-like particles (VLPs) (Cat# CBS-V088-C) were obtained from Creative Biostructures. Streptavidin from *S. avidinii* was obtained from either Sigma Aldrich (Cat# S0677) or Thermo

Fisher Scientific (Cat# 434302). Streptavidin R-phycoerythrin conjugate (SAPE) (Cat#S866) was obtained from Invitrogen.

2.2. Instrumentation

A Harvard PHD ULTRA™ pump was used to flow reagents through the system during chamber functionalization as well as device operation. Electrical measurements were made using a H2FLI lock-in amplifier and a HF2CA current amplifier from Zurich Instruments (Switzerland). A schematic of the measurement set-up can be seen in Fig. S1.† Off-chip data acquisition was done using the Moxi Go II cell counter (Orflo, USA). On-chip data acquisition was done using Labview 2013 (National Instruments, USA) and data analysis was performed with MATLAB (Mathworks, USA). Shear stress analysis of the capture chamber was performed using COMSOL Multiphysics.

2.3. Plasma samples

Pooled human plasma was obtained from Innovative Research (USA) (Cat# IPLAK2E10ML) and stored in aliquots at −20 °C.

2.4. Fabrication of capture chambers and functionalization

A master mold was prepared for the PDMS capture chamber using standard photolithography techniques with SU8-2050 negative photoresist on a 4 in Si wafer with a feature height of 55 μm. PDMS prepolymer and curing agent (Dow SYLGARD™ 184 Silicone Elastomer) were mixed in a 10 : 1 ratio, degassed, and cured overnight at 60 °C. Cured devices were then cut out from the molds, cut into individual devices, and punched with a 0.75 mm biopsy punch (Robbins Instruments). The PDMS capture chambers were activated alongside glass slides using oxygen plasma (2 min) and bonded together by pressing the activated surfaces together to form covalent bonds and heating them on a hot plate (15 min, 95 °C).

All six chambers that composed the set were functionalized in series after being connected by tubing. First the chambers were flushed by injecting 70% ethanol by hand to remove air, and then the ethanol was replaced by PBS by pumping PBS through at 50 μL min^{-1} for 4 min. Streptavidin was infused (400 μg mL^{-1}, 15 μL min^{-1}) until 50 μL were pumped and then incubated at room temperature for 30 min. This was repeated an additional time and then the chambers were blocked by infusing 250 μL of BSA solution (1% w/v in PBS) at a rate of 30 μL min^{-1} and then incubating at room temperature for at least 1 hour. Any additional reagent leftover in the chambers was flushed with PBS while connecting the chambers to the counter electrodes before acquiring data.

2.5. Fabrication of counter electrodes

Microfabricated co-planar gold electrodes were fabricated for the electrical counting as described previously.[24] A PDMS flow channel was prepared by creating a master mold using standard photolithography techniques with SU8-25 negative photoresist on Si wafers to obtain a feature height of 15 μm. The PDMS channel was bonded onto the electrodes utilizing APTES/GPTMS chemistry.[32] The channels and electrodes were aligned during bonding such that thinner portions of the channel (the apertures) were positioned between the electrodes, with each electrode set being composed of 3 electrodes in sequence (Fig. S2a†). Electrodes were then bound to a PCB board using silver conductive epoxy. Electrodes measures the impedance changes caused by beads flowing through the aperture between the electrodes using a Wheatstone bridge by acquiring output voltages across a 10 kΩ resistor (Fig. S2b†).

2.6. Synthesis of hydrogel beads

To synthesis each hydrogel bead population, a concentrated polyacrylamide stock solution (~85% T) was prepared by dissolving 0.0113 g bis-acrylamide, 0.02 g acryloyl β-alanine, and 0.1937 g acrylamide in 500 μL 40% BioRad stock containing 19 : 1 acrylamide : bis-acrylamide. Acryloyl β-alanine, which incorporates carboxylic acid groups into the polymerized particles (Fig. 2a), was synthesized following an established method and confirmed by ^{1}H NMR.[33] The stock was diluted to 55% T and 80% T in 0.5× PBS to make HB1 and HB2 respectively (Fig. 2b). Ammonium persulfate is included at 2 w/v% for HB1 and 0.5 w/v% for HB2. Each aqueous pre-gel solution was partitioned into monodisperse drops in 2% fluorosurfactant (RAN biotechnologies) in HFE-7500 oil (3 M) using a microfluidic dropmaker. The flow rates used for HB1 and HB2 were 25 : 65 μL h^{-1} and 15 : 30 μL h^{-1} aq : oil, respectively. The collected drops were polymerized during overnight incubation at 85 °C (HB1) or 55 °C (HB2). The resulting hydrogel beads were washed into 1× PBS where they swell to a final diameter of 13.28 ± 0.70 μm and 14.83 ± 0.76 μm (for HB1 and HB2 respectively). Gel bead images are shown in Fig. 2c and d. Due to the differences in gel content, HB1 and HB2 result in distinctive impedances pulses when measured on a Coulter counter (Fig. 2e).

2.7. Hydrogel beads functionalization

Antibodies were functionalized onto the hydrogel beads using carbodiimide coupling chemistry. The beads were washed in MES buffer: 2-(*N*-morpholino)ethansulfonic acid (0.1 M, pH 6). The beads were then resuspended in 10 mM 1-ethyl-3-(3-dimethylaminopropyl)-carbodiimide (EDC) with 5 mM *N*-hydroxysulfosuccinimide (NHS) in MES and mixed for 20 min to activate the carboxyl groups on the beads. The beads were then centrifuged and resuspended in PBS (pH 7.4), then centrifuged again. At this point, beads were resuspended in antibody solution in PBS : HB1 was resuspended in capture antibody for HAV (100 μg mL^{-1}, Creative Diagnostics Cat# DMABT-51306MH); HB2 was resuspended in B19V VP2 protein capture antibody (500 μg mL^{-1}, LifeSpan Biosciences Cat# LS-C371157-100). The beads were then incubated (3 h, 950 rpm), with beads being resuspended by pulsing every 30 minutes to prevent the beads from settling due to gravity. The beads were the centrifuged and washed with PBS, then resuspended in a 0.1% BSA and 75 μg mL^{-1} glycine solution and incubated again (2 h, 950 rpm) to block any remaining unbound carboxyl groups. Then, the beads were centrifuged and resuspended in BlockAid™ blocking solution (100 μL, Thermofisher) and stored at 4 °C. The final bead concentration

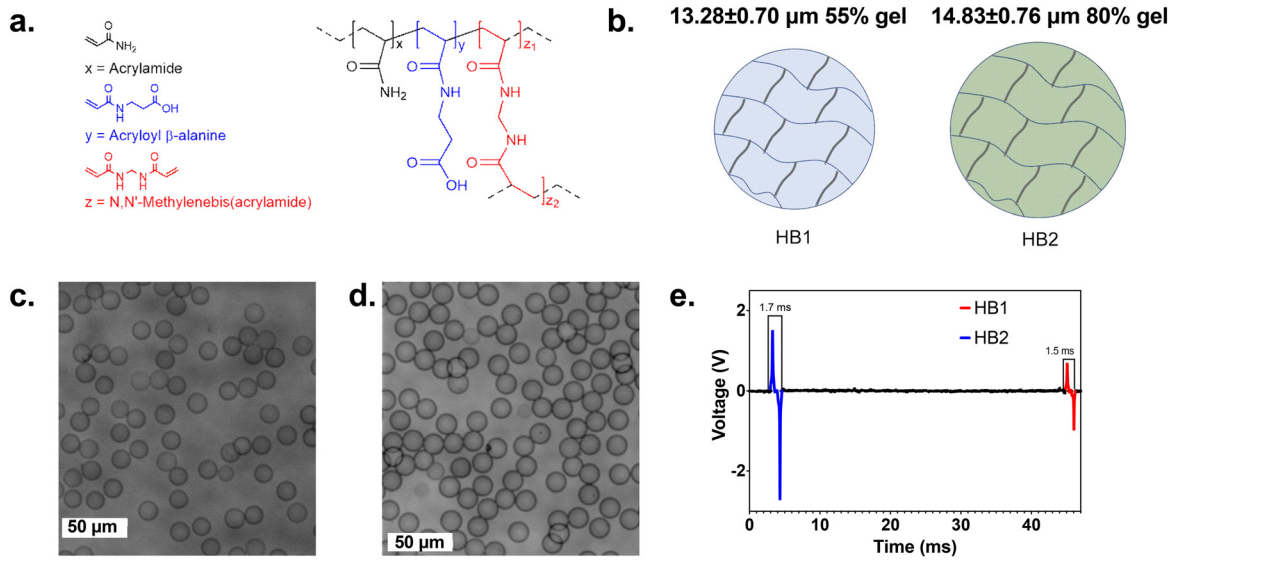

Fig. 2 Hydrogel beads. (a) Chemical structure; (b) diameter and gel content. Beads produce electrical impedance signals that increases with size and gel density of the beads; (c) and (d) microscope image of (c) HB1 and (d) HB2 beads after synthesis; (e) electrical impedance signals of HB1 and HB2 in sequence. The higher density and size of HB2 produce a larger electrical signal and ratio of signal lengths is roughly the same as the ratio of bead diameters.

after functionalization was measured using a Moxi GO II Coulter counter (ORFLO), and each was adjusted to 10 000 beads per μL by dilution in BlockAid™. Functionalized beads were stored at 4 °C for up to a month.

2.8. Sandwich immunoassay for virus detection

Sandwich immunoassays were performed in order to detect the presence of the target viruses (Fig. 1). Thus, for the assay we mixed the sample (75 μL, spiked buffer or spiked plasma) with a solution of biotinylated detection antibody to a reaction volume of 298 μL (when doing multiplexed detection) or 299 μL (when doing single virus detection) (10 μg mL^{-1}, LifeSpan Biosciences Cat# LS-C526508-100 for HAV and LifeSpan Biosciences Cat# LS-C371159-100 for B19V). Formaldehyde-inactivated full HAV particles (Creative Diagnostics Cat# DAG178) and B19V VLPs (Creative Biostructures Cat# CBS-V088-C) were used as targets for HAV and B19V respectively. This solution was pre-incubated (10 min, 950 rpm). Then the capture antibody-beads solution was added (1 μL, HB1-HAVab1, HB2-B19Vab1, or both for the multiplexed assays) to a final reaction volume of 300 μL. The solution was incubated (40 min, 950 rpm). After, PBS (300 μL) was added.

2.9. Acquisition of off-chip measurements

The products of the sandwich immunoassay were centrifuged and resuspended in PBS (500 μL) to wash, before being centrifuging again and resuspending in PBS (291 μL). Streptavidin R-phycoerythrin conjugate (SAPE, 9 μL, 1 mg mL^{-1}, Invitrogen Cat#S866) was then added and the solution was incubated (950 rpm, 30 min in darkness). After the incubation the solution was centrifuged and resuspended in PBS twice, with the final resuspension bringing the volume back to 300 μL. The resulting solution was vortexed and then measured with three replicates for each sample on the Moxi Go II system using the flow cytometry mode and the PE filter (561 nm/Long Pass) with fluorescence gain set to low. The size distribution was used to identify the bead signal from noise and the mean fluorescence intensity was taken across all beads within this range.

2.10. Acquisition of electrical measurements

The experimental procedure for the on-chip acquisition of the microfluidic differential counter has been described in detail previously.[24] Briefly, the final solution from the immunoassay step (200 μL) was loaded into a syringe and pumped through the system (20 μL min^{-1}, 5 min), going from the entrance electrode (entrance count), through the capture chamber, and then through the exit electrode (exit count). The sigmoidal bipolar impedance pulses were generated by applying a 303 kHz signal to the center electrodes of each set (entrance and exit) and measuring the impedance pulse amplitudes generated through the other two electrodes on the set as the beads flowed between them and the center electrode. This data was sampled at 250 kHz and processed in a custom MATLAB code (Fig. S2c and d†). This code filtered out noise using a 20 Hz high pass filter, a 303 kHz low pass filter, and 60 Hz and 120 Hz band stop filters for power line interference. The code then generated a histogram of the peak voltages to count the beads.

2.11. Statistical analysis

Statistical analysis was performed using GraphPad Prism 9 software. Mean fluorescent intensity and percentage of capture results from off-chip and on-chip tests respectively were recorded in the software, and the software was then used to

perform statistical analysis to compare between different concentrations of the viral target within each test. We chose to use *t*-tests for comparison since we can assume the factors that affect capture should be normally distributed, and since the standard deviation for the results cannot be assumed to be the same for each virus concentration, we applied the Welch's correction. We started by applying one-sided *t*-tests comparing the positives to the negatives to determine if positive samples produced a significantly higher response than negative samples. Then we tested two-sided *t*-tests between populations to determine the extent to which quantitative analysis could be performed between positive samples with different viral loads.

3. Results and discussion

3.1. Platform for the multiplexed detection of viral particles

The proposed platform aims to achieve specific capture of beads that had captured viruses through the use of the sandwich immunoassay protocol described in section 2.8., where in the presence of viruses, beads would form a sandwich complex consisting of a bead conjugated to the primary antibody, the virus, and a biotinylated secondary antibody. The immunoassay would be performed, then the resulting solution would be flowed through an entrance electrode which performs a count on all beads entering the capture chamber. The capture chambers were functionalized with streptavidin in advance as described in the section 2.4., protocol so that we could take advantage of the affinity between streptavidin and biotin to specifically capture the beads that had formed the sandwich complex with the virus and secondary antibody. Beads that were not captured this way would then flow out of the capture chamber outlet and into an exit electrode, where they would be counted. By taking the difference between entrance and exit counts, we can determine the number of beads that had been captured and calculate a percentage of capture that is correlated to the presence of virus in the initial sample. This entire process takes place in the span of under an hour, with 50 minutes for the immunoassay and 5 minutes of measurement (Fig. 1).

While the overall protocol remains similar to what was used in past work with this platform[23–25] adjustments were made to accommodate the unique challenges presented by working with whole viruses. Due to the presence of multiple target proteins on each virus particle, it is necessary for a preincubation with biotinylated detection antibody before the introduction of the hydrogels beads in order to partially block the available binding sites on each virus particle for the capture antibodies on the beads and prevent the formation of large aggregates capable of clogging up the chip that could occur if multiple beads bound to the same virus particles (Fig. S3†). The presence of these large aggregates when forgoing the preincubation led to high levels of electrode clogging that made collection of data for positive samples unviable. By adjusting the protocol to first include a short preincubation step with the viruses and secondary antibodies before introducing the beads, we were able to limit the number of binding sites still available on each virus that was accessible to the antibodies on the beads thus reducing the rate of aggregation. Additionally, by diluting the beads by half after the reaction time was done, we can reduce the bead concentration without affecting the assay time and allow for any aggregates that do still form to be less likely to cause major clogging and device failure.

Compared to our previous work with hydrogel beads,[25] in this work we have synthesized new sets of hydrogel beads with higher gel content (Fig. 2). These higher gel content hydrogel beads enable higher signals and improve signal-to-noise ratio. Furthermore, because in this work we would not use the magnetic properties of the beads for separation or mixing purposes, we decided to forego the use of magnetic particles within the hydrogel beads. Since not including the nanometric magnetic particles within the hydrogel beads does not affect the size or mechanical properties of the beads, their capture performance was not affected.

The capture chamber consists of a PDMS device lined with rows of symmetrically distributed pillars staggered at a 0.33 ratio,[24] however a new capture chamber design was prepared for this study to be better optimized for the size of hydrogel beads (13–15 μm) compared to what we have used in our previous work.[25] In this new design the pillar diameter was 50 μm and spacing between pillars was 20 μm. The goal of this design was to increase the dimensions to account for the larger beads being used compared to earlier work, while still retaining similar flow parameters to ensure positive capture rates would remain similar. This design was simulated in COMSOL with a 2D laminar flow simulation to ensure shear stress remained within similar parameters to our prior designs (average shear rate around the pillars ~700 s^{-1} and a maximum shear rate around the pillars of about 5000 s^{-1}) in order to ensure a similar capture profile when tested experimentally (Fig. S4†).

3.2. Off-chip virus detection

We started by demonstrating the ability of our platform to detect viruses individually spiked into buffer. In place of active virus, we used chemically inactivated HAV and B19V VLPs as our targets. The VLPs were designed to mimic true viral particles and as such we will treat one VLP as equivalent to 1 IU of virus. To understand the performance of our assay, we performed the assays across multiple concentrations of each virus spiked in buffer in order to obtain a calibration curve. These concentrations were based on clinically relevant levels, with HAV being tested from 2×10^4 to 2×10^3 IU mL^{-1} based on the viral loads found inpatients averaging at around 10^3 copies per mL in all HAV patients with average viral load being over 10^4 copies per mL in more severe cases[34–36] and B19V being tested from 10^8 to 10^6 IU mL^{-1} based on the concentrations commonly found in symptomatic patients (>10^6 IU mL^{-1}).[9,37] A study of B19 seronegative plasma pool-recipients shown that only those recipients who received plasma containing $10^{7.5}$–$10^{8.5}$ copies per mL (19 recipients) became or seroconverted and 14 showed evidence of virus replication after 3 months.[38]

Additionally, negative controls were performed for both viruses using buffer that had not been spiked with any virus. First, we validated the assay by performing an off-chip assay using SAPE. The SAPE would bind to the biotin in the secondary antibodies after the assay was performed making the amount of fluorescence measured tied to the success of the assay, with high fluorescence levels based on the number of secondary antibodies, and by extension virus particles, on any given bead. Thus, by taking the mean fluorescence intensity (MFI) values across all beads measured in the solution, we can determine the success level of the assay. When this test was performed for HAV we found average MFI values of 48.1, 44.8, 38.0, 37.1, 19.7 and 21.5 for 2×10^4, 1×10^4, 8×10^3, 4×10^3, 2×10^3, and 0 IU mL^{-1} respectively. When performed for B19V we found average MFI values of 1820, 756.7, 459.3 and 72.83 for 1×10^8, 1×10^7, 1×10^6, and 0 IU mL^{-1} respectively. For both viruses we found that all the positives were significantly different from the controls when compared with one-sided Welch's *t*-tests with the exception of 2×10^3 IU mL^{-1} of HAV (Fig. 3). Additionally, we were not able to get significantly different results between the positive results of the same virus at different concentrations tested for HAV, meaning that only a qualitative positive/negative result could be obtained from this assay and range of concentrations. However, for B19V while we could not get significantly different results between 10^6 and 10^7 IU mL^{-1}, we were able to get significantly different results between those two concentrations and the results for 10^8 IU mL^{-1}, meaning some level of quantification of viral loads is possible within the ranges tested using this assay.

3.3. On-chip individual virus detection

The assays were then repeated with the same concentrations on-chip using our differential counting system in order to validate and quantify the results of the assay using our platform. The results for HAV (Fig. 4a, c and S5†) showed that all positives were distinguishable from the negative controls when compared with a one-sided Welch's *t*-test, with mean percentage of capture of positives being 16.6%, 22.0%, 28.1%, 34.4%, and 30.1% capture for 2×10^3, 4×10^3, 8×10^3, 1×10^4, and 2×10^4 IU mL^{-1} of inactivated HAV virus to around compared to a mean nonspecific capture rate of 3.2% in the negative controls. However, the positives were not able to achieve significantly different rates of capture from each other, meaning that this test is only able to distinguish between positive and negative cases in clinically relevant ranges and cannot be used for quantitative analysis of viral load at this range. This is mainly due to the fact that only an order of magnitude separates the highest positive concentration tested from the lowest positive concentration tested. The result for B19V (Fig. 4b, d and S6†) showed capture rates of 48.0%, 71.2%, and 96.6% for 10^6, 10^7, and 10^8 VLP per mL respectively compared to 4.0% for the negative control. All three tested positive concentrations were not only statistically significant from the negative control but were all statistically significant from their neighboring concentrations as well using a two-sided Welch's *t*-test, meaning the test could allow for a quantitative assay of B19V concentrations. The lower rates of capture for HAV compared to B19V are likely attributable to the lower viral loads being tested. Additionally, when comparing the on and off-chip results, the on-chip tests show a greater sensitivity for HAV being able to obtain statistically significant differences between 2×10^3 IU mL^{-1} samples, and better differentiation between positive samples is achieved for B19V where we were able to obtain statistically significant differences between different levels of positives that was not possible in the off-chip assay. We hypothesize the reason for this improvement in capture is due to the formation of bead chains during the assay process (bead-Ab-virus-Ab-bead). While the pre-incubation step is designed to reduce the formation of large chains (large chains could clog the microfluidic channels), some bead chains will still form in

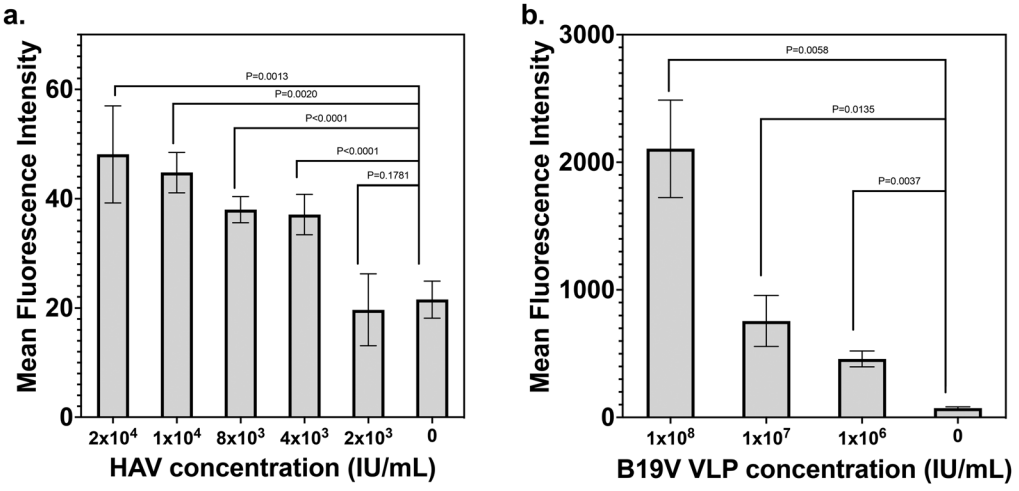

Fig. 3 Off-chip tests of individual virus assays in buffer. Bar plots showing mean fluorescence of beads read by flow cytometer after undergoing SAPE treatment for (a) HAV assay and (b) B19V assay. *P*-Values indicate results of one-sided Welch's *t*-test against negative control. Replicates per condition, $n = 3$.

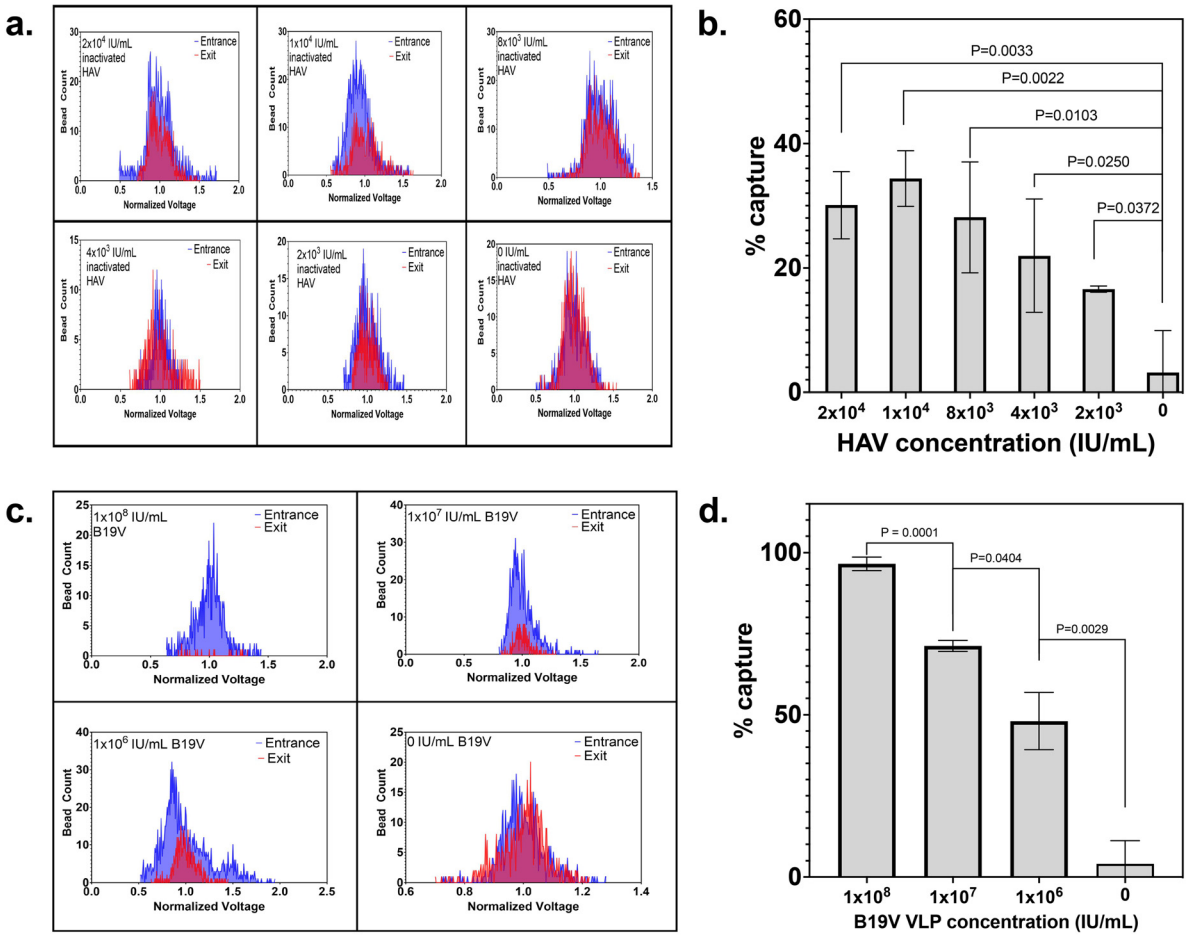

Fig. 4 On-chip individual virus assays in buffer. Overlaid entrance and exit counts histograms for (a) HAV and (b) B19V (additional replicates can be found in Fig. S5 and S6,† respectively). Blue area indicates entrance count, red area indicates exit count. Voltages are normalized against the average voltage signal of counts; bar plot showing capture rates with $n = 3$ replicates for (c) HAV and (d) B19V across tested concentrations. *P*-Values indicate results of one-sided Welch's *t*-test against negative control for (c) and 2-sided Welch's *t*-tests between consecutive concentrations for (d).

the presence of virus. These bead chains lead to another avenue of specific capture that is tied to the presence of the specific virus targets but is independent of the capture caused by the streptavidin–biotin interactions that are being tested in the off-chip assays.

Although currently there is no routine laboratory test to diagnose B19V infection,[39] PCR and VP1 and VP2 antigen tests can be used for detection of this virus.[9] Our device shows the ability to detect concentrations similar to those detected by other antigen tests for B19V (>10^6 IU mL^{-1}).[9] Similarly, HAV diagnostic tests is made by the detection of HAV-specific IgM antibodies or virus RNA (RT-PCR),[28] and our device shows the ability to detect concentrations similar to those detected in sera from blood samples taken from patients infected with HAV at different times after the onset of the disease (>10^3 IU mL^{-1}).[36]

3.4. On-chip multiplexed virus detection in plasma samples

Next, we demonstrated our platform capacity for achieving multiplexed detection of both viruses spiked in plasma samples. The lowest tested concentrations from the previous steps were used as positive samples (2×10^3 IU mL^{-1} for HAV; 10^6 IU mL^{-1} for B19V, both spiked in plasma samples), and all possible combinations of positives with those concentrations and negative controls (+/+, +/−, −/+, and −/−: HAV/B19V) for each virus were tested with 3 replicates each (Fig. 5 and S7†). The negative controls are virus-free plasma samples. The average percentages of capture for HAV were 16.8%, 14.8%, 5.0%, and 1.8% for the +/+, +/−, −/+, and −/− samples respectively. The average percentages of capture for B19V were 29.4%, 9.4%, 20.0%, and 3.0% for the +/+, +/−, −/+, and −/− samples respectively. The results showed a significant difference between each positive test and the negative controls from the −/− plasma samples when compared using a one-sided Welch's *t*-test. It is worth noting that while HAV capture rates in the multiplexed assay in plasma stayed consistent with the individual tests in buffer, B19V capture rates were significantly lower than the same concentrations tested alone in buffer. This may indicate that the B19V assay is more sensitive to inhibitors in the plasma sample. Additionally, when one bead

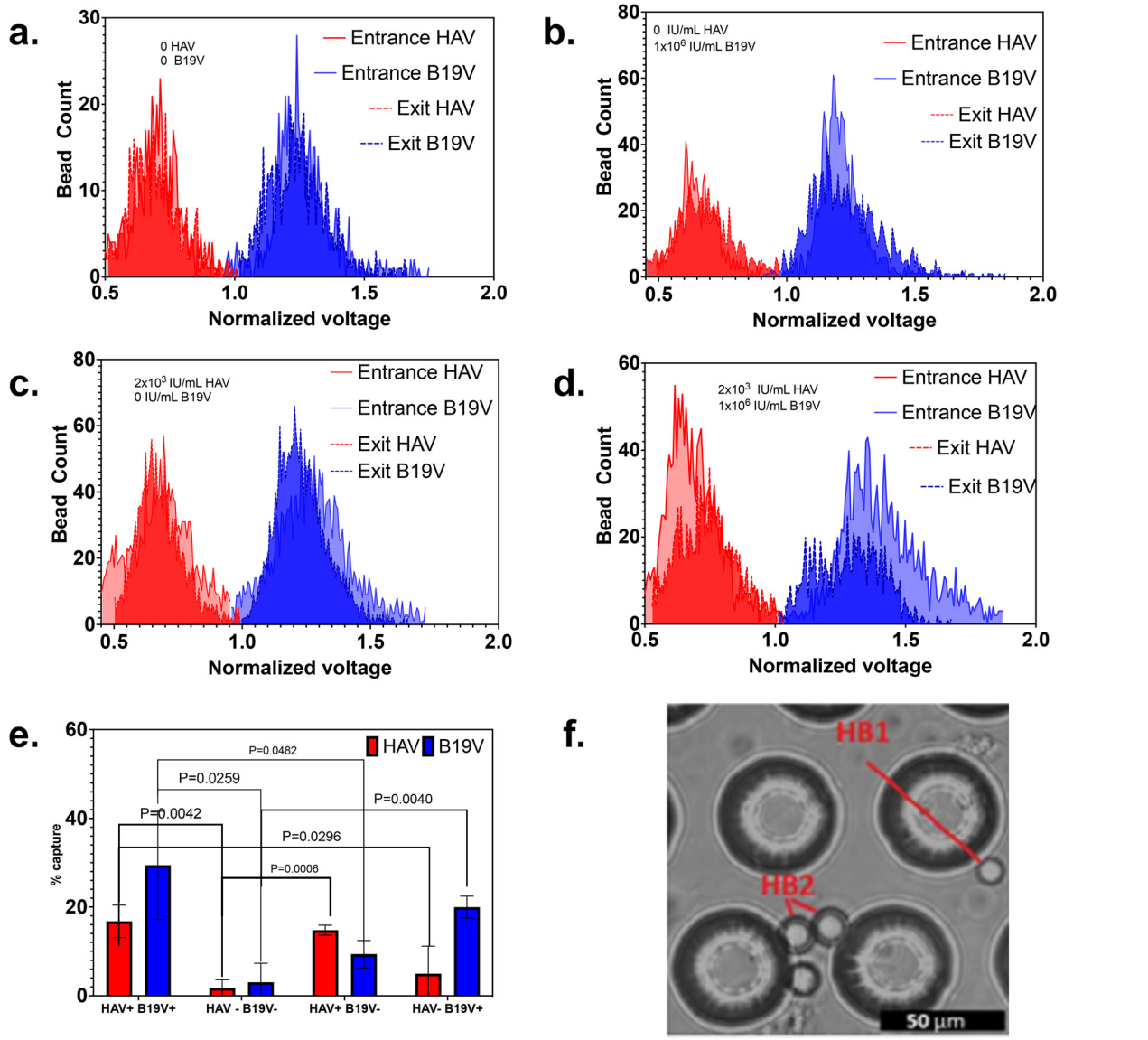

Fig. 5 Multiplexed virus detection in plasma. Overlaid entrance and exit counts for (a) −/− sample with 0 IU mL^{-1} HAV and 0 VLP per mL B19V; (b) −/+ sample with 0 IU mL^{-1} HAV and 10^6 VLP per mL B19V; (c) +/− sample with 2×10^3 IU mL^{-1} HAV and 0 VLP per mL B19V; (d) +/+ sample with 2×10^3 IU mL^{-1} HAV and 10^6 VLP per mL B19V. HAV is indicated in red, B19V in blue. Other replicates are included in Fig. S7.† Voltages are normalized against average voltage signal of counts; (e) bar plot showing multiplex capture results with $n = 3$ replicates across all tested combinations. *P*-Values indicate results of one-sided Welch's *t*-tests between positives and negatives for respective viruses; (f) microscope image of multiplexed capture in capture chamber from +/+ test.

type was captured, the non-specific capture rate for the other bead type seemed to go up when compared to when only one bead was present. This is likely due to blockage of the flow paths in the chamber that can occur when the capture rate of a bead type is high, which might be resolved with further optimization of the capture chamber in the future with multiplexing in mind. However, even if with this effect, the non-specific capture was well distinguishable from positive samples.

This represents to the best of our knowledge the first demonstration of multiplexed capture and detection of whole viral particles. Our platform is a screening device capable to clearly distinguishing between positive and negative samples at clinically relevant levels similar to what antibody tests can detect.[9,34–37] This will open up a range of applications where the detection of individual viral proteins may be misleading or unfeasible. Furthermore, because this technology has already been demonstrated to work with individual protein and nucleic acid targets,[23,25] and because the detection and capture within the device is reliant on streptavidin–biotin interactions that can be used for a variety of targets, it is capable of easily switching out targets for a more versatile and customizable assay without interfering with the results of the individual assays, as long as the target-specific antibodies are

available and do not have cross-reactivity issues. The ability to achieve multiplexed capture in a single chamber that is not functionalized specifically for the targets in question also increases the flexibility of the platform to switch between different assays compared to other multiplexed platforms that rely on compartmentalization with specific binding agents for each target functionalized beforehand to each compartment.[20,21] While several assays exist that achieve multiplexed detection of biomarkers on a single electrode by the use of electrochemical tags,[40–42] these have still relied on specific functionalization of the device to achieve specific detection. Additionally, while affinity-based electrochemical biosensors where the electrical signal comes from targets binding directly to electrode sensors can suffer issues from biofouling.[43,44] Importantly, our platform has been shown to work with lysed whole blood where detection is based on Coulter counting and the sample passing over the electrodes is in constant flow.[26]

4. Conclusions

Our electrical counting platform was successfully able to expand its library of targets and achieve multiplexed capture of whole viruses in plasma samples. We were able to demonstrate individual capture of each virus in buffer at a range of clinically relevant concentrations and demonstrate the ability to achieve multiplex capture and distinguish positive samples of both viruses at the lowest target concentrations tested within this range from negative controls. In the future, there are several areas that still need to be expanded on. In particular, we plan to demonstrate higher levels of multiplexing that are possible with this platform in combination with the use of our hydrogel beads. Both hydrogel beads used in this paper had higher gel contents than what we used in our previous work,[25] and thus they have higher electrical signals. Therefore, combining different similar sizes (in the order of 11–15 μm) with different gel contents we expect to further increase our multiplexing capabilities. Additionally, since the intent of this device is to be used at point-of-care, work must be done to incorporate the entire assay from mixing to detection onto an integrated portable device.

Author contributions

Aaron Jankelow: conceptualization; data curation; formal analysis; investigation; methodology, software; writing – original draft. Chih-Lin Chen: data curation; formal analysis; investigation; methodology; writing – original draft. Thomas W. Cowell: data curation; formal analysis; investigation; methodology; writing – review & editing. Javier Espinosa de los Monteros: investigation; Zheng Bian: investigation. Victoria Kindratenko: investigation; software. Katherine Koprowski: investigation. Sriya Darsi: investigation. Hee-Sun Han: conceptualization; funding acquisition; project administration; supervision; writing – review & editing. Enrique Valera: conceptualization; funding acquisition; project administration; supervision; writing – review & editing. Rashid Bashir: conceptualization; funding acquisition; project administration; supervision; writing – review & editing.

Conflicts of interest

R. B. is the co-founder of Prenosis, Inc. and VedaBio, Inc. but declares no conflicts with the work reported in this paper.

Acknowledgements

E. V., H.-S. H., and R. B. acknowledge support from the National Institutes of Health (R01AI148385). E. V., H.-S. H., and R. B. acknowledge financial support provided by CSL Behring. A. J., E. V. and R. B. acknowledge support from the Jump Applied Research through Community Health through Engineering and Simulation (ARCHES) endowment through the Health Care Engineering Systems Center at the UIUC. We also thank the NMR laboratory at the School of Chemical Sciences and the MechSE Cleanroom at the University of Illinois at Urbana-Champaign for their technical support.

References

1 A. Cassedy, A. Parle-McDermott and R. O'Kennedy, Virus detection: A review of the current and emerging molecular and immunological methods, *Front. Mol. Biosci.*, 2021, 76.
2 M. Wang, H. Liu, J. Ren, Y. Huang, Y. Deng, Y. Liu, *et al.* Enzyme-Assisted Nucleic Acid Amplification in Molecular Diagnosis: A Review, *Biosensors*, 2023, **13**(2), 160.
3 A. M. Jankelow, H. Lee, W. Wang, T.-H. Hoang, A. Bacon, F. Sun, *et al.*, Smartphone clip-on instrument and microfluidic processor for rapid sample-to-answer detection of Zika virus in whole blood using spatial RT-LAMP, *Analyst*, 2022, **147**, 3838–3853.
4 O. Mayboroda, I. Katakis and C. K. O'Sullivan, Multiplexed isothermal nucleic acid amplification, *Anal. Biochem.*, 2018, **545**, 20–30.
5 T. J. Moehling, G. Choi, L. C. Dugan, M. Salit and R. J. Meagher, LAMP diagnostics at the point-of-care: Emerging trends and perspectives for the developer community, *Expert Rev. Mol. Diagn.*, 2021, **21**(1), 43–61.
6 J. Y. Sim, L.-Y. Chang, J.-M. Chen, P.-I. Lee, L.-M. Huang and C.-Y. Lu, Human parvovirus B19 infection in patients with or without underlying diseases, *J. Microbiol., Immunol. Infect.*, 2019, **52**(4), 534–541.
7 L. O. Attwood, N. E. Holmes and L. Hui, Identification and management of congenital parvovirus <scp>B19</scp> infection, *Prenatal Diagn.*, 2020, **40**(13), 1722–1731.
8 N. S. Young and K. E. Brown, Parvovirus B19, *N. Engl. J. Med.*, 2004, **350**(6), 586–597.

9 M. F. Beersma, E. C. Claas, T. Sopaheluakan and A. C. Kroes, Parvovirus B19 viral loads in relation to VP1 and VP2 antibody responses in diagnostic blood samples, *J. Clin. Virol.*, 2005, **34**(1), 71–75.
10 A. Jones, L. Dhanapala, R. N. T. Kankanamage, C. V. Kumar and J. F. Rusling, Multiplexed Immunosensors and Immunoarrays, *Anal. Chem.*, 2020, **92**(1), 345–362.
11 A. M. Salama, G. Yasin, M. Zourob and J. Lu, Fluorescent biosensors for the detection of viruses using graphene and two-dimensional carbon nanomaterials, *Biosensors*, 2022, **12**(7), 460.
12 K. R. Mitchell, J. E. Esene and A. T. Woolley, Advances in multiplex electrical and optical detection of biomarkers using microfluidic devices, *Anal. Bioanal. Chem.*, 2022, **414**(1), 167–180.
13 N. A. Tanner, Y. Zhang and T. C. Evans Jr., Simultaneous multiple target detection in real-time loop-mediated isothermal amplification, *Biotechniques*, 2012, **53**(2), 81–89.
14 W. Chen, H. Chen, Y. Liu, H. Wei, Y. Wang, Z. Rong, *et al.*, An integrated fluorescent lateral flow assay for multiplex point-of-care detection of four respiratory viruses, *Anal. Biochem.*, 2022, **659**, 114948.
15 J.-H. Lee, H. S. Seo, J.-H. Kwon, H.-T. Kim, K. C. Kwon, S. J. Sim, *et al.*, Multiplex diagnosis of viral infectious diseases (AIDS, hepatitis C, and hepatitis A) based on point of care lateral flow assay using engineered proteinticles, *Biosens. Bioelectron.*, 2015, **69**, 213–225.
16 S. Y. Yi, J. Kwon, J. H. Lee, K. Yoon, Y. B. Shin and K. Park, Rapid and Simultaneous Detection of Dengue and Chikungunya Viruses by a Multiplex Lateral Flow Assay Using Ficolin-1, One of Human Innate Immune Defense Proteins, *J. Bacteriol. Virol.*, 2022, **52**(1), 1–10.
17 L. Chen, L. Song, Y. Zhang, P. Wang, Z. Xiao, Y. Guo, *et al.* Nitrogen and sulfur codoped reduced graphene oxide as a general platform for rapid and sensitive fluorescent detection of biological species, *ACS Appl. Mater. Interfaces*, 2016, **8**(18), 11255–11261.
18 F. Sassa, G. C. Biswas and H. Suzuki, Microfabricated electrochemical sensing devices, *Lab Chip.*, 2020, **20**(8), 1358–1389.
19 G. C. Biswas, S. Choudhury, M. M. Rabbani and J. Das, A Review on Potential Electrochemical Point-of-Care Tests Targeting Pandemic Infectious Disease Detection: COVID-19 as a Reference, *Chemosensors*, 2022, **10**(7), 269.
20 J.-H. Han, D. Lee, C. H. C. Chew, T. Kim and J. J. Pak, A multi-virus detectable microfluidic electrochemical immunosensor for simultaneous detection of H1N1, H5N1, and H7N9 virus using ZnO nanorods for sensitivity enhancement, *Sens. Actuators, B*, 2016, **228**, 36–42.
21 R. M. Torrente-Rodríguez, H. Lukas, J. Tu, J. Min, Y. Yang, C. Xu, *et al.*, SARS-CoV-2 RapidPlex: a graphene-based multiplexed telemedicine platform for rapid and low-cost COVID-19 diagnosis and monitoring, *Matter*, 2020, **3**(6), 1981–1998.
22 H. Yousefi, A. Mahmud, D. Chang, J. Das, S. Gomis, J. B. Chen, *et al.*, Detection of SARS-CoV-2 Viral Particles Using Direct, Reagent-Free Electrochemical Sensing, *J. Am. Chem. Soc.*, 2021, **143**(4), 1722–1727.
23 J. Berger, E. Valera, A. Jankelow, C. Garcia, M. Akhand, J. Heredia, *et al.*, Simultaneous electrical detection of IL-6 and PCT using a microfluidic biochip platform, *Biomed. Microdevices*, 2020, **22**(2), 36.
24 E. Valera, J. Berger, U. Hassan, T. Ghonge, J. Liu, M. Rappleye, *et al.*, A microfluidic biochip platform for electrical quantification of proteins, *Lab Chip*, 2018, **18**(10), 1461–1470.
25 T. W. Cowell, E. Valera, A. Jankelow, J. Park, A. W. Schrader, R. Ding, *et al.*, Rapid, multiplexed detection of biomolecules using electrically distinct hydrogel beads, *Lab Chip*, 2020, **20**(13), 2274–2283.
26 U. Hassan, T. Ghonge, B. Reddy, M. Patel, M. Rappleye, I. Taneja, *et al.*, A point-of-care microfluidic biochip for quantification of CD64 expression from whole blood for sepsis stratification, *Nat. Commun.*, 2017, **8**(1), 15949.
27 U. Hassan, N. N. Watkins, B. Reddy, G. Damhorst and R. Bashir, Microfluidic differential immunocapture biochip for specific leukocyte counting, *Nat. Protoc.*, 2016, **11**(4), 714–726.
28 World-Health-Organization. Hepatitis A 2022 [available from: **https://www.who.int/news-room/fact-sheets/detail/hepatitis-a**.
29 A. Wolfromm, C. Rodriguez, M. Michel, A. Habibi, V. Audard, E. Benayoun, *et al.*, Spectrum of adult Parvovirus B19 infection according to the underlying predisposing condition and proposals for clinical practice, *Br. J. Haematol.*, 2015, **170**(2), 192–199.
30 D. I. Stuart, J. Ren, X. Wang, Z. Rao and E. E. Fry, Hepatitis A Virus Capsid Structure, *Cold Spring Harbor Perspect. Med.*, 2019, **9**(5), a031807.
31 B. Kaufmann, A. A. Simpson and M. G. Rossmann, The structure of human parvovirus B19, *Proc. Natl. Acad. Sci. U. S. A.*, 2004, **101**(32), 11628–11633.
32 L. Tang and N. Y. Lee, A facile route for irreversible bonding of plastic-PDMS hybrid microdevices at room temperature, *Lab Chip*, 2010, **10**(10), 1274.
33 I.-D. Chung, P. Britt, D. Xie, E. Harth and J. Mays, Synthesis of amino acid-based polymers via atom transfer radical polymerization in aqueous media at ambient temperature, *Chem. Commun.*, 2005, (8), 1046.
34 K. Fujiwara, H. Kojima, S. Yasui, K. Okitsu, Y. Yonemitsu, M. Omata, *et al.*, Hepatitis A viral load in relation to severity of the infection, *J. Med. Virol.*, 2011, **83**(2), 201–207.
35 H. W. Lee, D.-Y. Chang, H. J. Moon, H. Y. Chang, E.-C. Shin, J. S. Lee, *et al.*, Clinical Factors and Viral Load Influencing Severity of Acute Hepatitis A, *PLoS One*, 2015, **10**(6), e0130728.
36 A. Normann, C. Jung, A. Vallbracht and B. Flehmig, Time course of hepatitis A viremia and viral load in the blood of human hepatitis A patients, *J. Med. Virol.*, 2004, **72**(1), 10–16.
37 M. L. Landry, Parvovirus B19, *Microbiol. Spectrum*, 2016, **4**(3), DOI: **10.1128/microbiolspec.DMIH2-0008-2015**.

38 K. E. Brown, N. S. Young, B. M. Alving and L. H. Barbosa, Parvovirus B19: implications for transfusion medicine. Summary of a workshop, *Transfusion*, 2001, **41**(1), 130–135.
39 CDC. Parvovirus Symptoms and Complications 2023 [October 18, 2023]. Available from: **https://www.cdc.gov/parvovirusb19/symptoms-complications.html**.
40 M. Sharafeldin and J. F. Rusling, Multiplexed electrochemical assays for clinical applications, *Curr. Opin. Electrochem.*, 2023, **39**, 101256.
41 L.-N. Feng, Z.-P. Bian, J. Peng, F. Jiang, G.-H. Yang, Y.-D. Zhu, *et al.*, Ultrasensitive Multianalyte Electrochemical Immunoassay Based on Metal Ion Functionalized Titanium Phosphate Nanospheres, *Anal. Chem.*, 2012, **84**(18), 7810–7815.
42 Y. Li, Y. Chang, J. Ma, Z. Wu, R. Yuan and Y. Chai, Programming a target-initiated bifunctional DNAzyme nanodevice for sensitive ratiometric electrochemical biosensing, *Anal. Chem.*, 2019, **91**(9), 6127–6133.
43 E. Valera, V. Kindratenko, A. M. Jankelow, J. Heredia, A. Y. Kim, T. W. Cowell, *et al.*, Electrochemical point-of-care devices for the diagnosis of sepsis, *Curr. Opin. Electrochem.*, 2023, 101300.
44 J. Sabaté del Río, O. Y. F. Henry, P. Jolly and D. E. Ingber, An antifouling coating that enables affinity-based electrochemical biosensing in complex biological fluids, *Nat. Nanotechnol.*, 2019, **14**(12), 1143–1149.

